

Cesium $nD_J + 6S_{1/2}$ Rydberg molecules and their permanent electric dipole moments

Suying Bai,^{1,2,*} Xiaoxuan Han,^{1,2,*} Jingxu Bai,^{1,2} Yuechun Jiao,^{1,2} Jianming Zhao^{1,2,†}, Suotang Jia,^{1,2} and Georg Raithel³

¹State Key Laboratory of Quantum Optics and Quantum Optics Devices, Institute of Laser Spectroscopy, Shanxi University, Taiyuan 030006, China

²Collaborative Innovation Center of Extreme Optics, Shanxi University, Taiyuan 030006, China

³Department of Physics, University of Michigan, Ann Arbor, Michigan 48109-1120, USA

 (Received 14 February 2020; revised 23 May 2020; accepted 8 September 2020; published 30 September 2020)

Cs_2 Rydberg-ground molecules consisting of a Rydberg, nD_J ($33 \leq n \leq 39$), and a ground-state atom, $6S_{1/2}$ ($F = 3$ or 4), are investigated by photo-association spectroscopy in a cold atomic gas. We observe vibrational spectra that correspond to triplet $^T\Sigma$ and mixed $^{S,T}\Sigma$ molecular states. We establish scaling laws for the energies of the lowest vibrational states vs principal quantum number and obtain zero-energy singlet and triplet s -wave scattering lengths from experimental data and a Fermi model. Line broadening in electric fields reveals the permanent molecular electric-dipole moments. Measured values agree well with calculations, which also reveal that the dipole moments are negative. The negative sign reflects a deficiency of Rydberg-electron density near the ground-state perturber, which is caused by electronic configuration mixing. The mixing leads to destructive wave function interference near the perturber. This case differs from previous reports of positive dipole moments, where the interference near the perturber is constructive.

DOI: [10.1103/PhysRevResearch.2.033525](https://doi.org/10.1103/PhysRevResearch.2.033525)

Recently, molecules formed between a ground-state and a Rydberg atom have attracted considerable attention due to their rich vibrational level structure and permanent electric-dipole moments, which are unique for homonuclear molecules. A Rydberg-ground molecule arises from low-energy scattering between the Rydberg electron and ground-state atoms located inside the Rydberg electron's wave function. This interaction, initially investigated in Refs. [1,2], has been predicted to lead to molecular binding in a novel type of Rydberg molecules, including the so-called trilobite [3] and butterfly molecule [4,5]. The molecular bond length is on the order of the Rydberg-atom size (a thousand Bohr radii a_0). Rydberg-ground molecules were first reported in experiments with Rb $nS_{1/2}$ ($n = 35\text{--}37$) states [6] and later with Rb $nP_{1/2,3/2}$ [7] and $nD_{3/2,5/2}$ [8–10] states, as well as with Cs $nS_{1/2}$ [11,12], $nP_{3/2}$ [13], and $nD_{3/2}$ [14] states. Ultralong-range blueshifted Cs_2 molecular states near $nS_{1/2}$ Rydberg states were reported in Ref. [11]. The permanent electric-dipole moment of S -type Rydberg-ground molecules has been measured to be ≈ 1 Debye for Rb [15] and a few thousand Debye for Cs [12]. The large size and the permanent electric-dipole moments of Rydberg-ground molecules make these molecules good candidates for the realization of certain strongly correlated many-body gases [16] and for quantum

information processing [17–19], as well as for dipolar quantum gases and spin systems with long-range interactions [20,21].

Here we report on the measurement of long-range Cs_2 ($nD_J + 6S_{1/2}F$) Rydberg-ground molecules for $33 \leq n \leq 39$, $J = 3/2$ or $5/2$, and $F = 3$ or 4 . These molecules are deeply in the Hund's case-(c) regime, which differs from Rb $nD_{3/2,5/2}$ -type molecules at lower n , which are Hund's case (a) [10] or between Hund's case (a) and (c) [8,9]. Using a Fermi model, we calculate molecular potential-energy curves (PECs), vibrational energies, and permanent electric-dipole moments of Cs_2 ($nD_{5/2} + 6S_{1/2}F$) Rydberg molecules. The dipole moments are found to be negative, with the negative sign being attributed to destructive interference of the Rydberg electron wave function near the perturber. This differs from previously reported cases of positive dipole moments [11–13,22], where the interference near the perturber is constructive.

The scattering interaction between the Rydberg electron and the ground-state atom is, in the reference frame of the Rydberg ionic core [2],

$$\hat{V}(\mathbf{r}; R) = 2\pi a_s(k)\delta^3(\mathbf{r} - R\hat{\mathbf{z}}) + 6\pi [a_p(k)]^3 \delta^3(\mathbf{r} - R\hat{\mathbf{z}}) \overleftarrow{\nabla} \cdot \overrightarrow{\nabla}, \quad (1)$$

where \mathbf{r} and $R\hat{\mathbf{z}}$ are the positions of the Rydberg electron and the perturber atom, $a_l(k)$ are the scattering lengths, k is the electron momentum, and l is the scattering partial-wave order (0 or 1 for s wave or p wave, respectively). The full Hamiltonian of the system is [23]

$$\hat{H}(\mathbf{r}; R) = \hat{H}_0 + \sum_{i=S,T} \hat{V}(\mathbf{r}; R)\hat{P}(i) + A_{HFS}\hat{\mathbf{S}}_2 \cdot \hat{\mathbf{I}}_2, \quad (2)$$

*These authors contributed equally to this work.

†zhaojm@sxu.edu.cn

Published by the American Physical Society under the terms of the Creative Commons Attribution 4.0 International license. Further distribution of this work must maintain attribution to the author(s) and the published article's title, journal citation, and DOI.

where \hat{H}_0 is the unperturbed Hamiltonian, which includes the spin-orbit interaction of the Rydberg atom. The second term sums over singlet ($i = S$) and triplet ($i = T$) scattering channels, using the projection operators $\hat{P}(T) = \hat{\mathbf{S}}_1 \cdot \hat{\mathbf{S}}_2 + 3/4$, $\hat{P}(S) = 1 - \hat{P}(T)$ ($\hat{\mathbf{S}}_1$ and $\hat{\mathbf{S}}_2$ are the electronic spins of the Rydberg and ground-state atom, respectively). The last term represents the hyperfine coupling of $\hat{\mathbf{S}}_2$ to the ground-state-atom nuclear spin $\hat{\mathbf{I}}_2$, with hyperfine parameter A_{HFS} . Numerical solutions of the Hamiltonian in Eq. (2) on a grid of R values yield sets of PECs. Figure 1(a) shows four PECs that are asymptotically connected with the atomic $36D_{5/2}$ state. The PECs for ${}^T\Sigma$ for $6S_{1/2}F = 3$ and $F = 4$ are practically identical, while the PECs for ${}^{S,T}\Sigma$ are ≈ 10 MHz deeper for $F = 3$ than for $F = 4$. A similar behavior was seen in Rb [8,10] and Cs [13].

The experiment is performed in a crossed optical dipole trap (CODT) loaded from a magneto-optical trap (MOT). The CODT density, measured by absorption imaging, is $\approx 10^{11}$ cm $^{-3}$. This is sufficiently dense to excite Rydberg-ground molecules with bond lengths ≈ 0.12 μm (our case). After switching off the trapping lasers, two counterpropagated 852 and 510 nm lasers (pulse duration 3 μs) are applied to photo-associate the atoms into Rydberg-ground molecules. The lasers are both frequency stabilized to the same high-finesse Fabry-Perot (FP) cavity to less than 500 kHz linewidth. The 852 nm laser is 360 MHz blue-detuned from the intermediate $|6P_{3/2}, F' = 5\rangle$ level. The 510 nm laser is scanned from the atomic Rydberg line to ≈ 150 MHz below by scanning the radio-frequency signal (rf) applied to the electro-optic modulator used to lock the laser to the FP cavity. Rydberg molecules are formed when the detuning from the atomic line matches the binding energy of a molecular vibrational state. Rydberg molecular (atomic) ions are produced by Hornbeck-Molnar autoionization (blackbody photoionization) and detected with a microchannel plate (MCP) detector. Suitable timing of the MOT repumping laser allows us to prepare the atoms and molecules in either $F = 4$ or $F = 3$. The 510 nm laser can be tuned to excite either $nD_{5/2} + 6S_{1/2}$ or $nD_{3/2} + 6S_{1/2}$ molecules.

In Fig. 1 we show photo-association spectra of $36D_{5/2} + 6S_{1/2}$ molecules for $F = 4$ [Fig. 1(b)] and $F = 3$ [Fig. 1(c)], respectively. To reduce uncertainties, the spectra are averaged over ten measurements. Both spectra display a pair of dominant molecular peaks, marked with triangles. They correspond to the vibrational ground ($\nu = 0$) states in the outermost wells of the shallow (${}^{S,T}\Sigma$) and deep (${}^T\Sigma$) PECs shown in Fig. 1(a), which arise from s -wave scattering. The deep, ${}^T\Sigma$ PEC corresponds with a triplet state of the Rydberg electron and the $6S_{1/2}$ atom. The two ${}^{S,T}\Sigma$ PECs correspond with mixed singlet-triplet states and have a reduced depth, which is roughly in proportion to the amount of triplet character in the molecular states. The binding energies of the ${}^*\Sigma, \nu = 0$ states are extracted from Gaussian fits to the measured molecular peaks, with statistical uncertainties on the order of 1 MHz. Systematic uncertainties in the molecular line positions are negligible because of the high signal-to-noise ratio of the atomic reference lines in the spectra (relative to which the binding energies are measured), and because the FP cavity and the rf used to lock and scan the lasers have no significant drift.

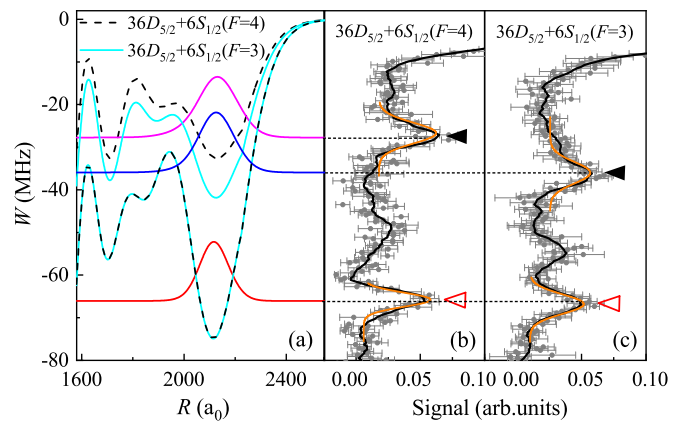


FIG. 1. (a) PECs for $36D_{5/2} + 6S_{1/2}(F = 4)$ (dashed lines) and $36D_{5/2} + 6S_{1/2}(F = 3)$ molecules (cyan solid lines), respectively. The deep potentials mostly arise from triplet s -wave scattering (${}^T\Sigma$) and do not depend on F . The shallow potentials mostly arise from s -wave scattering of mixed ${}^{S,T}\Sigma$ states and depend on F ; the PEC for ${}^{S,T}\Sigma$ $F = 3$ is deeper than that for ${}^{S,T}\Sigma$ $F = 4$. The colored lines show the $\nu = 0$ vibrational wave functions on the PECs. (b), (c) Experimental photo-association spectra for $36D_{5/2} + 6S_{1/2}(F = 4)$ and $36D_{5/2} + 6S_{1/2}(F = 3)$ molecules. Energies are relative to the respective $36D_{5/2}$ asymptotes. Filled (open) triangles mark the molecular signals formed by mixed ${}^{S,T}\Sigma$ (triplet ${}^T\Sigma$) potentials. Gray symbols and error bars show data points, black lines display smoothed averages. The error bars are the standard error of ten independent measurements. The thin yellow lines display Gaussian fittings.

We have obtained the photo-association spectra for all combinations of J and F , for $n = 33$ to 39. In Fig. 2 we show the results for the case $n = 36$. The ${}^T\Sigma, \nu = 0$ and ${}^{S,T}\Sigma, \nu = 0$ states are well resolved and allow for accurate comparison of level energies between experiment and theory. The ${}^T\Sigma, \nu = 0$ levels, marked by solid vertical lines, do not depend on F . Since the PECs for the measured states are largely due to s -wave scattering, the ratio of the binding energies of the ${}^T\Sigma, \nu = 0$ levels between $J = 3/2$ and $J = 5/2$ is approximately given by the square of the ratio between the Clebsch-Gordan coefficients $\langle J, m_j = 1/2 | m_\ell = 0, m_s = 1/2 \rangle$, with $J = 3/2$ or $5/2$, and with magnetic quantum numbers m_j, m_ℓ , and m_s for the coupled, orbital, and electron spins of the Rydberg electron, respectively. For D -type Rydberg-ground molecules in Hund's case (c), the binding-energy ratio is $\ell/(\ell + 1) = 2/3$, which is close to the binding-energy ratio evident in Fig. 2. The vertical dashed lines of Fig. 2 mark the ${}^{S,T}\Sigma, \nu = 0$ states, which are mixed singlet-triplet. These are about half as deeply bound as ${}^T\Sigma, \nu = 0$, whereby ${}^{S,T}\Sigma, \nu = 0$ for $F = 3$ is about 5 to 10 MHz more deeply bound than ${}^{S,T}\Sigma, \nu = 0$ for $F = 4$.

For quantitative modeling of the singlet and triplet s -wave scattering length functions $a_s^T(k)$ and $a_s^S(k)$, we have measured the binding energies of the states ${}^T\Sigma, \nu = 0$ and ${}^{S,T}\Sigma, \nu = 0$ for $nD_{5/2} + 6S_{1/2}$ molecules with $n = 33$ –39, for both values of F . The measured data, listed in detail in Table III in the Appendix, are fit with functions $an^{*b_{\text{Expt}}}$, with effective quantum number n^* and exponent b_{Expt} (see Table I). The b_{Expt} are concentrated around -5.60 , with one exception.

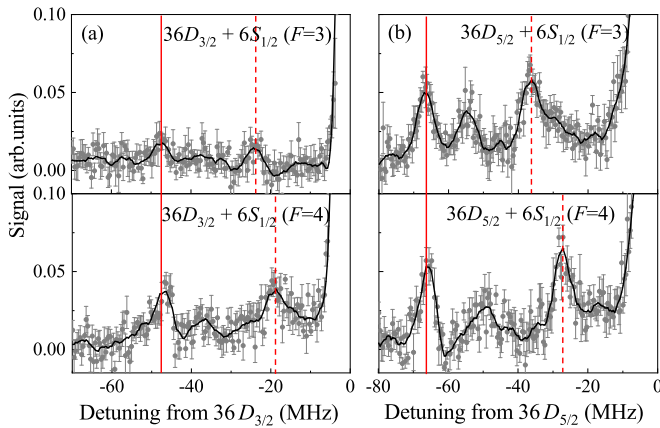


FIG. 2. Measured spectra of $36D_J + 6S_{1/2}$ molecules for (a) $J = 3/2$ and (b) $J = 5/2$, for (top) $F = 3$ and (bottom) $F = 4$. The laser detunings are relative to the atomic resonances, and the signal strengths are displayed on identical scales. Vertical solid and dashed lines mark the signals of the $^T\Sigma(v=0)$ and $^{S,T}\Sigma(v=0)$ ground vibrational states, respectively. The signal strengths of the $J = 5/2$ spectra are higher than those of the $J = 3/2$ ones, due to the higher excitation probability of the $nD_{5/2}$ atoms.

Calculated binding energies, also listed in Table III, yield respective fit exponents b_{Theor} that are within the uncertainty of the b_{Expt} (see Table I), with the exception of the $^{S,T}\Sigma F = 4$ case, where the binding energies are smallest. The b values generally have a magnitude that is significantly less than -6 . A value of -6 would be expected based on Rydberg wave-function density. The deviation of b from -6 may be attributed to the fact that at lower n the molecules are less deep in Hund's case (c) than at higher n . This may diminish the binding of the $J = 5/2$ molecules at lower n and lead to a reduction of the magnitude of b . A modification of the scaling may also arise from p -wave-scattering-induced configuration mixing at lower n as well as from the zero-point energy of the vibrational states.

The measured binding-energy data are employed to determine s -wave scattering lengths via comparison with model calculations similar to Ref. [10]. The calculations yield best-fitting s -wave scattering-length functions for both singlet and triplet scattering, $a_s^S(k)$ and $a_s^T(k)$, with zero-energy scattering lengths $a_s^S(k=0) = -1.92a_0$ and $a_s^T(k=0) = -19.16a_0$; a comparison with previous results is presented in Table IV in the Appendix. In our calculation we have included p -wave scattering and found that it has only a small effect on the lowest vibrational resonances in the outermost wells of the PECs [24], within our n range of interest. This is because

TABLE I. Fitted exponents b (see text) for the scaling of the binding energies of $^{S,T}\Sigma v = 0$ and $^T\Sigma v = 0$ states of $(nD_{5/2} + 6S_{1/2}F)$ molecules, for $F = 3$ and 4, over the range $33 \leq n \leq 39$. The fit function is an^{*b} , with effective quantum number n^* and exponent b .

	$S/T(F = 3)$	$T(F = 3)$	$S/T(F = 4)$	$T(F = 4)$
b_{Expt}	-5.65 ± 0.38	-5.60 ± 0.16	-6.19 ± 0.14	-5.62 ± 0.16
b_{Theor}	-5.68 ± 0.01	-5.62 ± 0.01	-5.55 ± 0.01	-5.62 ± 0.01

the outermost wells are separated fairly well from further-in wells and are therefore strongly dominated by s -wave scattering, justifying our use of less accurate nonrelativistic p -wave scattering-length functions $a_p^S(k)$ and $a_p^T(k)$ [25].

Homomuclear Rydberg-ground molecules are unusual, in part, because of their permanent electric-dipole moment d , which is caused by configuration mixing. The values of d are usually small in molecules with low- ℓ character, with the notable exception of Cs S -type molecules, where the quantum defect allows strong mixing with trilobite states [12]. The d value is usually positive [11–13,22], corresponding to an accumulation of Rydberg-electron density near the ground-state perturber atom. For the Cs nD -type Rydberg molecules in our work, we find a deficiency of electron density near the perturber, as detailed below.

The values of $d_{i,v}$, with index i denoting the PEC and v the vibrational state, can be measured via the broadening of the respective molecular line in an applied weak electric field, E . For electric-dipole energies, $-\mathbf{d}_{i,v} \cdot \mathbf{E}$, that are much smaller than the molecular binding energy, the line is inhomogeneously broadened about its center by a square function of full width $2d_{i,v}E/h$ in frequency. This model applies if the moment of inertia of Rydberg molecules is very large and rotational structure cannot be resolved (our case). The square function is convoluted with a Gaussian profile to account for laser line broadening, electric-field inhomogeneities, magnetic fields, etc. The standard deviation σ_f of this Gaussian is experimentally determined by fitting field-free molecular lines. The overall line profile, $S_{i,v}(\Delta f)$, as a function of detuning Δf from the line center is then

$$\frac{h}{2dE} \left[\text{erf} \left(\frac{\Delta f + d_{i,v}E/h}{\sqrt{2}\sigma_f} \right) - \text{erf} \left(\frac{\Delta f - d_{i,v}E/h}{\sqrt{2}\sigma_f} \right) \right]. \quad (3)$$

Since the field E is accurately known from Rydberg Stark spectroscopy, the values of $|d_{i,v}|$ follow from comparing measured lineshapes with profile functions calculated using Eq. (3) over a range of test values for $|d_{i,v}|$.

In Fig. 3 we show line-broadening measurements for $37D_{5/2} + 6S_{1/2}(F = 4)$ Rydberg molecules in several electric fields, as well as fit results based on Eq. (3) for the vibrational ground states of $^T\Sigma$ (top) and $^{S,T}\Sigma$ (bottom) PECs for the case $E = 0.37$ V/cm. The obtained dipole-moment magnitudes are $5.70ea_0$ ($6.34ea_0$) for the triplet (mixed) states. Analysis of the spectra for 0.18, 0.27, and 0.37 V/cm yields averaged dipole-moment magnitudes of $(4.79 \pm 0.78)ea_0$ for $^T\Sigma$ and $(5.49 \pm 1.03)ea_0$ for $^{S,T}\Sigma$.

For a comparison with theory, we first solve Eq. (2) to obtain the PECs and electronic adiabatic dipole moments along the internuclear axis, $d_{i,z}(R)$. We then find the vibrational energies and wave functions, $\Psi_{i,v}(R)$, on the PECs [23]. The dipole moments of the molecules, $d_{i,v}$, are

$$d_{i,v} = \int |\Psi_{i,v}(R)|^2 d_{i,z}(R) dR. \quad (4)$$

For the $^T\Sigma, v = 0$ states we find $d_{i,v}$ values ranging between $-4.85ea_0$ at $n = 33$ and $-4.60ea_0$ at $n = 38$. For $n = 37$, the calculated dipole moment is $-4.64ea_0$, which is in good agreement with the measured result [$|d| = (4.79 \pm 0.78)ea_0$].

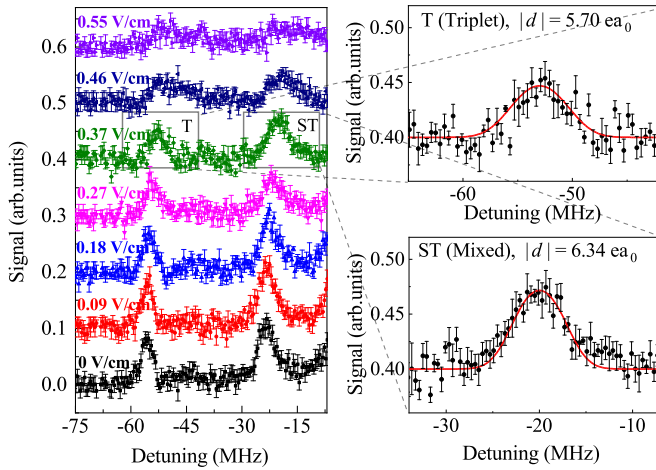


FIG. 3. Spectra of $37D_{5/2} + 6S_{1/2} (F = 4)$ Rydberg-ground molecules with indicated electric fields, E . The molecular peaks of $^T\Sigma, \nu = 0$ and $^{S,T}\Sigma, \nu = 0$ are blueshifted by E and substantially broadened in fields $E \geq 0.27$ V/cm. The right panel shows zoom-ins on the states $^T\Sigma (\nu = 0)$ (top) and $^{S,T}\Sigma (\nu = 0)$ (bottom). The red solid lines show model spectra based on Eq. (3) for dipole moments of magnitude $|d| = 5.70ea_0$ for $^T\Sigma, \nu = 0$ and $6.34ea_0$ for $^{S,T}\Sigma, \nu = 0$, respectively.

We note that the molecular lines also exhibit a DC Stark shift due to the electric polarizability α of the Rydberg atom. The atomic DC Stark shifts, $-\alpha_{m_j} E^2/2$, depend on the magnetic quantum number m_j due to the tensor component of the polarizability. If the molecular Stark shift is less than the molecular binding, it can be calculated perturbatively as an average shift with weights $P(m_j)$, where m_j is in the laboratory frame (defined by the direction of the applied electric field). Figure 3 further includes a hint that the molecular lines may split in stronger electric fields (top curve for 0.55 V/cm). The DC Stark shifts and possible splittings can result in an overestimate of the molecular dipole moment; this may explain the deviations between measured and calculated dipole moments.

While the current measurement method does not give the sign of $d_{i,v}$, the calculations reveal that the $d_{i,v}$ of Cs nD_J -type Rydberg-ground molecules are *negative*, which differs from reports on other types of Rydberg-ground molecules [11–13,22]. Physically, the sign of $d_{i,v}$ reflects the direction of the electronic charge shift along the axis of the Rydberg molecule relative to the location of the Cs $6S_{1/2}$ atom. The direction of the weak electric field E applied to measure the dipole moment is not relevant, as long as the field is weak (our case). A negative $d_{i,v}$ corresponds with a deficiency of electron charge from the vicinity of the Cs $6S_{1/2}$ perturber atom. This situation can generally be described as destructive interference of the Rydberg electron wave function near the perturber or, equivalently, as a destructive case of electronic configuration mixing near the perturber (linear combination of atomic orbitals picture).

For further illustration, in Fig. 4 we show electronic wave functions of Cs D -type and P -type Rydberg-ground molecules in the outer well of the respective PECs (see Fig. 1 for typical PECs). The projection of total angular momentum onto the molecular axis used in the presented calculation is $m_k = 2.5$.

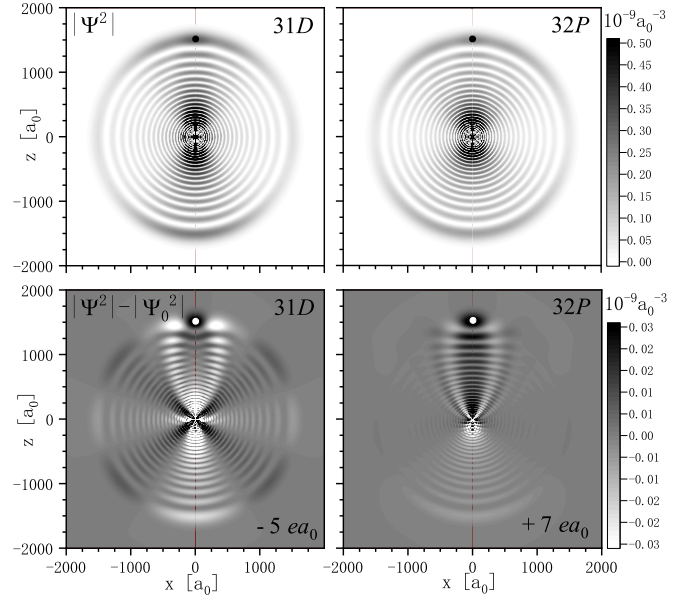


FIG. 4. Densities of adiabatic electronic wave functions for Cs $31D_{5/2} + 6S_{1/2} (F = 4)$ $^T\Sigma$ (left) and $32P_{3/2} + 6S_{1/2} (F = 4)$ $^T\Sigma$ (right panels), with the perturber located at $\approx 1500a_0$ (dot). (top) Wave function densities. (bottom) Difference between electronic wave function densities of molecules and atoms on a linear gray-scale, with white and black indicating reductions and increases by amounts shown on the gray-scale bar. The P -type molecular state (right) carries a trilobite-like component that interferes mostly constructively with the P -orbital, causing a positive dipole moment of about $7ea_0$. In the case of the D -type molecule (left), the trilobite orbital predominantly shows destructive interference with the D -orbital, causing a negative dipole moment of about $-5ea_0$.

Since the configuration mixing is weak, in the bottom panels in Fig. 4 we plot the difference of the wave-function density relative to that of the unperturbed atomic state. The admixture probabilities of electronic orbitals $|\ell, m_\ell\rangle$ to the D -type and P -type Rydberg-ground molecules is represented in Table II. Figure 4 and Table II show that the D -type molecule mostly mixes with P orbitals and with a combination of high- ℓ states similar to the trilobite state [3], while the P -type molecule mostly mixes with D orbitals and the trilobite-like orbital. The admixing from the trilobite orbital, denoted $[T, m_\ell = 0]$ in Table II, is strongest, and it is about twice as strong for the D -type molecule than it is for the P -type molecule. Admixtures from S and F states are smaller. The overall admixture probabilities are $\approx 10^{-4}$, corresponding to a typical wave function density variation on the order of a few percent, as seen in Fig. 4, leading to $|d_{i,v}|$ values much smaller than the wave-function diameter. In Fig. 4 it is seen that the P -state molecule exhibits predominantly constructive interference near the perturber, corresponding to a positive dipole moment. A similar mixing analysis was reported for Rb ($35S + 5S$) molecules with a small positive dipole moment [15]. Interestingly, for the D -state molecule in Cs, the mixing near the perturber results in a complex interference pattern that has constructive parts in the immediate vicinity of the perturber, as well as destructive parts at some distance away from the perturber. Overall, destructive interference dominates within the hemispherical

TABLE II. Admixture probabilities for D -type and P -type molecules from orbital-angular-momentum states $|\ell, m_\ell\rangle$ of the Rydberg electron, for projection of the total angular momentum onto the molecular axis of $m_k = 2.5$. The first four rows correspond to $\ell = 0$ to 3, while the last row signifies probability sums over $|\ell \geq 4, m_\ell\rangle$. The label T identifies the trilobite orbital.

D-type molecule			P-type molecule		
–	$ \text{S}, m_\ell = 0\rangle$ 7.90×10^{-7}	–	–	$ \text{S}, m_\ell = 0\rangle$ 5.70×10^{-7}	–
$ \text{P}, m_\ell = -1\rangle$ 3.28×10^{-6}	$ \text{P}, m_\ell = 0\rangle$ 2.19×10^{-5}	$ \text{P}, m_\ell = 1\rangle$ 1.15×10^{-5}	$ \text{P}, m_\ell = -1\rangle$ 0.074	$ \text{P}, m_\ell = 0\rangle$ 0.667	$ \text{P}, m_\ell = 1\rangle$ 0.259
$ \text{D}, m_\ell = -1\rangle$ 0.089	$ \text{D}, m_\ell = 0\rangle$ 0.599	$ \text{D}, m_\ell = 1\rangle$ 0.311	$ \text{D}, m_\ell = -1\rangle$ 6.21×10^{-6}	$ \text{D}, m_\ell = 0\rangle$ 2.91×10^{-5}	$ \text{D}, m_\ell = 1\rangle$ 2.17×10^{-5}
$ \text{F}, m_\ell = -1\rangle$ 6.02×10^{-7}	$ \text{F}, m_\ell = 0\rangle$ 2.83×10^{-6}	$ \text{F}, m_\ell = 1\rangle$ 2.11×10^{-6}	$ \text{F}, m_\ell = -1\rangle$ 4.36×10^{-7}	$ \text{F}, m_\ell = 0\rangle$ 2.05×10^{-6}	$ \text{F}, m_\ell = 1\rangle$ 1.53×10^{-6}
$ \ast, m_\ell = -1\rangle$ 2.60×10^{-5}	$ \text{T}, m_\ell = 0\rangle$ 1.18×10^{-4}	$ \ast, m_\ell = 1\rangle$ 9.09×10^{-5}	$ \ast, m_\ell = -1\rangle$ 1.53×10^{-5}	$ \text{T}, m_\ell = 0\rangle$ 6.90×10^{-5}	$ \ast, m_\ell = 1\rangle$ 5.34×10^{-5}

volume where the perturber is located ($z > 0$ in Fig. 4). The predominantly destructive interference on the perturber's side results in a negative dipole moment.

We have verified in calculations not shown that the dipole moments do not depend on the quantum number m_k . This independence is related to the fact that the probabilities in Table II for $|\ell, m_\ell = 0\rangle$ do not depend on m_k , and that the sums of probabilities over m_ℓ , for fixed ℓ , do not depend on m_k . Finally, we have confirmed with additional wave function calculations that the trilobite-like high- ℓ -superposition orbital that is admixed to the P - and D -type molecules is the same in both these cases. It is only the amplitude and the phase of the admixing that varies between the P - and D -type molecules, leading to different interference patterns as well as different dipole moments with opposite signs.

In summary, we have observed Cs nD Rydberg-ground molecules involving Rydberg-state fine structure and ground-state hyperfine structure. Measurements of the binding energies for ${}^T\Sigma(\nu = 0)$ and ${}^{S,T}\Sigma(\nu = 0)$ molecular vibrational states were modeled with calculations. We have measured permanent electric-dipole moments with magnitudes of a few ea_0 . Calculations show that the dipole moment is *negative*. The negative sign signifies a deficiency of Rydberg-electron wave-function density near the ground-state perturber, caused by destructive interference near the perturber. Future mea-

surements of both magnitude and sign of the dipole moment would add insight into possible varieties of the structure of Rydberg-ground molecules. Future work may further elucidate the exact behavior of molecular Stark shifts and splittings due to the tensor atomic polarizability, as well as the transition from weak to large electric-dipole energy shifts relative to the molecular binding.

The work was supported by the National Key R&D Program of China (Grant No. 2017YFA0304203), the National Natural Science Foundation of China (Grants No. 11434007, No. 61835007, No. 61675123, No. 61775124, and No. 11804202), Changjiang Scholars and Innovative Research Team in University of Ministry of Education of China (Grant No. IRT_17R70), and the 111 project (Grant No. D18001) and 1331KSC.

APPENDIX

1. Binding Energies of Vibrational Ground States

We have presented measurements and calculations of the binding energies of the states ${}^T\Sigma, \nu = 0$ and ${}^{S,T}\Sigma, \nu = 0$ for $n = 33$ –39 for both values of F for Cs ($nD_{5/2} + 6S_{1/2}F$) Rydberg-ground molecules. We have chosen the fine-structure component $J = 5/2$, because its molecular levels are more

TABLE III. Measurements and calculations of binding energies, in MHz, of ${}^{S,T}\Sigma, \nu = 0$ and ${}^T\Sigma, \nu = 0$ states of ($nD_{5/2} + 6S_{1/2}F$) Rydberg-ground molecules, for $F = 3$ and 4 and $33 \leq n \leq 39$. The binding energies are fit with allometric functions an^{*b} , with effective quantum number n^* and exponents b shown in the last row for each of the four measured and calculated data columns.

n	Measurements				Calculations			
	$S/T(F = 3)$	$T(F = 3)$	$S/T(F = 4)$	$T(F = 4)$	$S/T(F = 3)$	$T(F = 3)$	$S/T(F = 4)$	$T(F = 4)$
33	63.5 ± 1.5	114.0 ± 1.0	49.7 ± 1.0	112.0 ± 1.0	61.1	111.7	46.6	111.7
34	50.0 ± 1.0	95.0 ± 1.0	39.7 ± 0.5	94.7 ± 0.5	50.9	93.3	39.0	93.3
35	39.0 ± 1.0	76.0 ± 1.0	32.8 ± 0.5	75.8 ± 0.5	42.7	78.4	32.8	78.3
36	36.2 ± 1.5	66.5 ± 0.5	26.7 ± 1.0	66.0 ± 1.0	35.9	66.1	27.7	66.1
37	31.2 ± 1.5	58.2 ± 1.5	22.2 ± 0.5	56.2 ± 0.5	30.4	56.0	23.5	56.0
38	26.6 ± 1.5	49.5 ± 1.5	19.7 ± 0.5	48.2 ± 0.5	25.8	47.6	20.1	47.6
39	23.0 ± 1.0	43.0 ± 1.0	16.7 ± 1.0	42.0 ± 1.0	22.0	40.6	17.2	40.6
b	-5.65 ± 0.38	-5.60 ± 0.16	-6.19 ± 0.14	-5.62 ± 0.16	-5.68 ± 0.01	-5.62 ± 0.01	-5.55 ± 0.01	-5.62 ± 0.01

deeply bound than those of the $J = 3/2$ component, leading to a better relative uncertainty of the measured binding energies. The measured binding energies are shown in the left block of Table III. The values have uncertainties on the order of 1 MHz. We also display calculations of binding energies in the right block of Table III for comparison.

2. Model Data

The data in Table III have been employed to determine s -wave scattering lengths via comparison with model calculations similar to the one described in Ref. [10]. In the nonrelativistic approach, we have used finite-range model potentials for the low-energy electron-scattering provided in Ref. [25]. The s -wave singlet and triplet scattering wave functions of the electron were integrated numerically and evaluated at a distance of $1000a_0$ from the perturber to determine the scattering-length functions $a_s^S(k)$ and $a_s^T(k)$. This was done for electron wave numbers ranging from 0.0003 to 0.3000 in atomic units. These functions were then used to solve the Hamiltonian in Eqs. (1) and (2) of our paper, producing potential-energy curves (PECs), such as those shown in Fig. 1 of our paper. With the PECs calculated, it was possible to calculate the binding energies of the $\nu = 0$ vibrational resonances.

To achieve agreement between experimental and theoretical binding energies it was necessary to fine-tune the s -wave scattering-length functions $a_s^S(k)$ and $a_s^T(k)$. This was done by phase-shifting the wave function of the scattered electron by a small amount, at a small distance ($0.1a_0$) from the scattering center, while still using the finite-range model potentials from Ref. [25]. The shifts of the scattered-electron wave function were parametrized by the zero-energy scattering lengths, $a_s^S(k=0)$ and $a_s^T(k=0)$. We obtained the complete functions $a_s^S(k)$ and $a_s^T(k)$ on a grid of test values for $a_s^S(k=0)$ and $a_s^T(k=0)$, and used the complete functions $a_s^S(k)$ and $a_s^T(k)$ to calculate the molecular binding energies as described. We iteratively determined the values for $a_s^S(k=0)$ and $a_s^T(k=0)$ that yield the lowest overall deviation of calculated binding energies from the measured values in the left block in

TABLE IV. Theoretical (top block) and experimental (lower block) zero-energy scattering lengths reported in literature, in units of a_0 .

	$a_s^T(k=0)$	$a_s^S(k=0)$	Ref.
Theor.	-22.7	-2.40	[26]
	-21.7	-1.33	[27]
	-17		[28]
Expt.	-21.8 ± 0.2	-3.5 ± 0.4	[13]
	-20.71		[22]
	-19.16	-1.92	This work

Table III. This was done for principal quantum number $n = 36$. We found $a_s^S(k=0) = -1.92a_0$ and $a_s^T(k=0) = -19.16a_0$. The corresponding complete functions $a_s^S(k)$ and $a_s^T(k)$ were then used to calculate the binding energies. The absolute deviation between measured and calculated binding energies typically is $\lesssim 2.0$ MHz; the largest deviation of 3.7 MHz is seen for the $35D^{\text{S,T}}\Sigma, \nu = 0$ state. The average relative deviation between calculated and measured binding energies is 2.8%.

Note that, for the n range and the types of molecular states of interest in our paper, the p -wave scattering has a relatively small effect on the PECs over the range of the ground vibrational states in the outermost potentials. This is because, in our n range, the outermost wells are separated fairly well from further-in wells and are therefore strongly dominated by s -wave scattering. Therefore, for the p -wave scattering-length functions $a_p^S(k)$ and $a_p^T(k)$ we used nonrelativistic functions provided by Fabrikant *et al.* [25], without further adjustment.

We have fit experimental and calculated binding energies with allometric functions $\propto an^{*b}$, with effective quantum number n^* and exponent b . In the last line in Table III we list the fitting exponents b for both experimental and calculated data.

3. Zero-Energy s -Wave Scattering Lengths

For comparison with earlier work elsewhere, in Table IV we show the $a_s^S(k=0)$ and $a_s^T(k=0)$ values obtained in our present work and in the cited references.

-
- [1] E. Fermi, *Nuovo Cimento* **11**, 157 (1934).
 - [2] A. Omont, *J. Phys. (Paris)* **38**, 1343 (1977).
 - [3] C. H. Greene, A. S. Dickinson, and H. R. Sadeghpour, *Phys. Rev. Lett.* **85**, 2458 (2000).
 - [4] E. L. Hamilton, C. H. Greene, and H. R. Sadeghpour, *J. Phys. B: At., Mol. Opt. Phys.* **35**, L199 (2002).
 - [5] M. I. Chibisov, A. A. Khuskivadze, and I. I. Fabrikant, *J. Phys. B: At., Mol. Opt. Phys.* **35**, L193 (2002).
 - [6] V. Bendkowsky, B. Butscher, J. Nipper, J. P. Shaffer, R. Löw, and T. Pfau, *Nature (London)* **458**, 1005 (2009).
 - [7] M. A. Bellos, R. Carollo, J. Banerjee, E. E. Eyler, P. L. Gould, and W. C. Stwalley, *Phys. Rev. Lett.* **111**, 053001 (2013).
 - [8] D. A. Anderson, S. A. Miller, and G. Raithel, *Phys. Rev. Lett.* **112**, 163201 (2014).
 - [9] A. T. Krupp, A. Gaj, J. B. Balewski, P. Ilzhöfer, S. Hofferberth, R. Löw, T. Pfau, M. Kurz, and P. Schmelcher, *Phys. Rev. Lett.* **112**, 143008 (2014).
 - [10] J. L. MacLennan, Y. J. Chen, and G. Raithel, *Phys. Rev. A* **99**, 033407 (2019).
 - [11] J. Tallant, S. T. Rittenhouse, D. Booth, H. R. Sadeghpour, and J. P. Shaffer, *Phys. Rev. Lett.* **109**, 173202 (2012).
 - [12] D. Booth, S. T. Rittenhouse, J. Yang, H. R. Sadeghpour, and J. P. Shaffer, *Science* **348**, 99 (2015).
 - [13] H. Saßmannshausen, F. Merkt, and J. Deiglmayr, *Phys. Rev. Lett.* **114**, 133201 (2015).
 - [14] C. Fey, J. Yang, S. T. Rittenhouse, F. Munkes, M. Baluktsian, P. Schmelcher, H. R. Sadeghpour, and J. P. Shaffer, *Phys. Rev. Lett.* **122**, 103001 (2019).

- [15] W. Li, T. Pohl, J. M. Rost, S. T. Rittenhouse, H. R. Sadeghpour, J. Nipper, B. Butscher, J. B. Balewski, V. Bendkowsky, R. Löw, and T. Pfau, *Science* **334**, 1110 (2011).
- [16] H. Weimer, M. Müller, I. Lesanovsky, P. Zoller, and H. P. Büchler, *Nat. Phys.* **6**, 382 (2010).
- [17] M. D. Lukin, M. Fleischhauer, R. Cote, L. M. Duan, D. Jaksch, J. I. Cirac, and P. Zoller, *Phys. Rev. Lett.* **87**, 037901 (2001).
- [18] D. DeMille, *Phys. Rev. Lett.* **88**, 067901 (2002).
- [19] P. Rabl, D. DeMille, J. M. Doyle, M. D. Lukin, R. J. Schoelkopf, and P. Zoller, *Phys. Rev. Lett.* **97**, 033003 (2006).
- [20] M. A. Baranov, M. Dalmonte, G. Pupillo, and P. Zoller, *Chem. Rev. (Washington, DC, US)* **112**, 5012 (2012).
- [21] H. Kadau, M. Schmitt, M. Wenzel, C. Wink, T. Maier, I. Ferrier-Barbut, and T. Pfau, *Nature (London)* **530**, 194 (2016).
- [22] S. Markson, S. T. Rittenhouse, R. Schmidt, J. P. Shaffer, and H. R. Sadeghpour, *ChemPhysChem* **17**, 3683 (2016).
- [23] D. A. Anderson, S. A. Miller, and G. Raithel, *Phys. Rev. A* **90**, 062518 (2014).
- [24] S. Bai, X. Han, J. Bai, Y. Jiao, H. Wang, J. Zhao, and S. Jia, *J. Chem. Phys.* **152**, 084302 (2020).
- [25] A. A. Khuskivadze, M. I. Chibisov, and I. I. Fabrikant, *Phys. Rev. A* **66**, 042709 (2002).
- [26] I. I. Fabrikant, *J. Phys. B: At. Mol. Phys.* **19**, 1527 (1986).
- [27] C. Bahrim, U. Thumm, and I. I. Fabrikant, *J. Phys. B: At., Mol. Opt. Phys.* **34**, L195 (2001).
- [28] C. Bahrim and U. Thumm, *Phys. Rev. A* **61**, 022722 (2000).